Annu. Rev. Biophys. Biomol. Struct. 1994. 23:247–85

BIOLOGICAL APPLICATIONS OF OPTICAL FORCES

Karel Svoboda

Committee on Biophysics, Harvard University, Cambridge, Massachusetts 02138 and Rowland Institute for Science, 100 Edwin Land Boulevard, Cambridge, Massachusetts 02142

Steven M. Block

Rowland Institute for Science, 100 Edwin Land Boulevard, Cambridge, Massachusetts 02142 and Department of Molecular Biology, Princeton University, Princeton, New Jersey 08544

KEY WORDS: optical tweezers, optical trapping, radiation pressure, lasers, tensiometry

---

CONTENTS

1056–8700/94/0610–0247$05.00

PERSPECTIVES AND OVERVIEW

In the first part of the seventeenth century, the German astronomer Johannes Kepler proposed that the reason comet tails point away from the sun is because they are pushed in that direction by the sun's radiation. In his theory of electromagnetism of 1873, James Clerk Maxwell showed theoretically that light itself can exert optical force, or *radiation pressure,* but this was not demonstrated experimentally until the turn of the century. One reason for the lapse of nearly three centuries between hypothesis and verification is that radiation pressure is extraordinarily feeble. Milliwatts of power (corresponding to very bright light) impinging on an object produce piconewtons of force (1 pN = 10^{-12} N). The advent of lasers in the 1960s finally enabled researchers to study radiation pressure through the use of intense, collimated sources of light. An early pioneer of such studies was Arthur Ashkin of AT&T (Bell) Laboratories. By focusing laser light down into narrow beams, Ashkin and others demonstrated that tiny particles, such as polystyrene spheres a few micrometers in diameter, could be displaced and even levitated against gravity using the force of radiation pressure (1–3, 5, 6, 66). Ashkin's work on the effects of radiation pressure laid much of the groundwork for the development of laser-based atom trapping and cooling methods employed by today's physicists (2a, 33, 34).

One particular optical trapping scheme, proposed in 1978 and demonstrated in 1986 (2a, 10), simply consisted of bringing a beam of laser light to a diffraction-limited focus using a good lens, such as a microscope objective. Under the right conditions, the intense light gradient near the focal region can achieve stable three-dimensional trapping of dielectric objects. Optical traps employing this design do not trap atoms at room temperature, but they can be used to capture and remotely manipulate a wide range of larger particles, varying in size from several nanometers up to tens of micrometers. The term *optical tweezers* was coined to describe this single-beam scheme. In many respects, it resembles a scaled-down version of the tractor beam of popular science fiction. Ashkin and coworkers showed in 1987 that optical tweezers could manipulate living, as well as inanimate, material and that through proper choice of wavelength, optical damage to biological specimens could be minimized. Employing a continuous-wave (cw) near-infrared laser (Nd:YAG , λ = 1064 nm), Ashkin captured viruses, yeasts, bacteria, and protozoa (7, 11). Experiments in other laboratories during the past few years have begun to explore the rich possibilities afforded by optical trapping in biology. Although still in their infancy, laser-

based optical traps have already had significant impact, mainly because they afford an unprecedented means to manipulate on the microscopic scale.

Optical forces are miniscule on the scale of larger organisms, but they can be significant on the scale of macromolecules, organelles, and even whole cells. A force of ten piconewtons, equal to one microdyne, can tow a bacterium through water faster than it can swim, halt a swimming sperm cell in its track, or arrest the transport of an intracellular vesicle. A force of this magnitude can also stretch, bend, or otherwise distort single macromolecules, such as DNA and RNA, or macromolecular assemblies, including cytoskeletal components such as microtubules and actin filaments. Mechanoenzymes such as myosin, kinesin, and dynein produce forces in the piconewton range. Optical traps are therefore especially well suited to studying mechanics or dynamics at the cellular and subcellular levels.

Recent reviews have covered the scope of the first generation of biological experiments (8, 20, 22, 23, 46, 54, 74, 88). The present discussion concentrates instead on current developments. It also deals with related technical issues, including a critique of optical trapping theory, considerations for instrument design and calibration, and novel approaches to using optical forces. Finally, we hope to communicate our sense of future directions for this growing field.

TRAPPING BASICS

Optical traps use radiation pressure, a term that refers generally to forces imparted to matter by the absorption, scattering, emission, or reradiation of light (i.e. by photons). Radiation pressure may manifest itself in several ways. Perhaps the most familiar form is the *scattering force,* which, following current usage, is defined as that force due to light scattering that is proportional to the light intensity and acts in the direction of propagation of light. This force may also be regarded as a consequence of the momentum delivered by the scattered photons. Optical tweezers, however, owe their trapping to the *gradient force,* which is instead proportional to the spatial gradient in light intensity and acts in the direction of that gradient. Other optical forces include, for example, the *optical binding force,* which is an interaction between particles in intense light (30, 31). All optical forces arise from the same physics.

The gradient force used by optical tweezers arises from fluctuating electric dipoles that are induced when light passes through transparent objects, which consequently experience a time-averaged force in the

direction of the field gradient. When an object's dimensions are substantially greater than the wavelength of light, i.e. when $d \gg \lambda$, a condition referred to as the Mie regime, a simple ray-optic picture suffices to explain the phenomenon (Figure 1). Rays of light carry momentum and are bent by refraction when passing through a dielectric sphere with a refractive index, n, greater than the surrounding medium. By conservation of momentum, the rate of change of momentum in the deflected rays conveys an equal and opposite rate of change in mo-

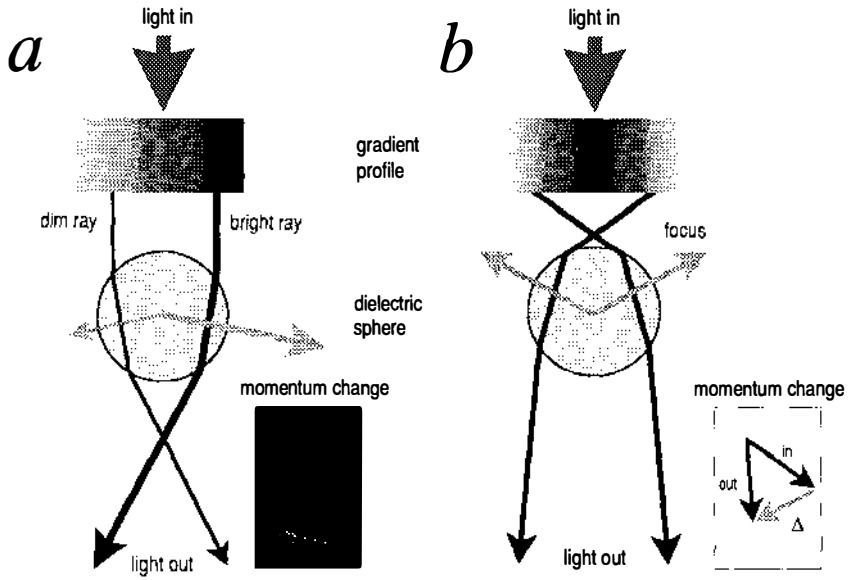

Figure 1 (*a*) A ray-optic picture of the gradient force. A parallel beam of light (*large gray arrow*) with a gradient in intensity (*shaded region;* the darker color indicates more light) shines through a transparent sphere with a higher refractive index than its background. The relative thickness of the two representative rays (*black arrows*) symbolizes intensity. The rays are refracted, giving rise to the reaction forces shown acting through the sphere's center (*gray arrows*). The brighter right ray conveys more force than the dimmer left ray: the sum of all rays in the beam tends to pull the sphere rightwards towards the light. (*Inset*) A vector diagram indicating the change of momentum for the right ray. The difference in momentum (*gray arrow*) produces an equal and opposite reaction in the sphere. (*b*) A single beam trap. Light (*large gray arrow*) is brought to a focus: its beam profile has an intensity gradient (*shaded region*). Two representative rays (*black arrows*) pass through a transparent sphere located beyond the focus. The rays are bent, and reaction forces (*gray arrows*) pull the sphere upwards, towards the focus. (*Inset*) A vector diagram indicating the change of momentum in the left ray. The difference in momentum (*gray arrow*) produces an equal and opposite reaction in the sphere.

mentum to the sphere. The rate of change of momentum produces a force by Newton's Second Law.

When a dielectric sphere is placed in a light gradient, the sum of all rays passing through it generates an imbalance in force, tending to push the sphere towards the brighter region of the light. A focus functions as a trap because the strong light gradients in its neighborhood all point towards the center. Trapping is stable when the gradient force in the region beyond the focus is adequate to overcome the scattering force, which would otherwise propel the object out of the trap's center along the optical axis. This condition occurs, in practice, only with the steepest possible light gradients, e.g. those produced by a microscope objective of high numerical aperture (NA).

In the Rayleigh regime, where $d \ll \lambda$, light cannot be represented by rays, but trapping still occurs, and the magnitude of the trapping force is proportional to the field gradient. In this regime, objects can be represented as point dipole scatterers, simplifying theory. However, a focus cannot be represented as a point, but as a diffraction-limited region whose overall dimensions are close to λ. Unfortunately, most biological work falls into the intermediate regime ($d \approx \lambda$), where no dimensions can be neglected and calculations become difficult. Biological specimens further confound matters by tending to be nonspherical and inhomogeneous with respect to refractive index. Because of these complications, optical trapping theory is relatively immature. These and other considerations are discussed in greater detail in the trapping theory section of this review.

RECENT EXPERIMENTS

Optical traps have many intriguing applications (for reviews, see 8, 20, 22, 23, 46, 54, 74, 88). Ashkin & Dzeidzic used optical forces to stretch plant cell membranes into slender filaments to study their viscoeleastic properties (9). In collaboration with M Schliwa's group, they also used optical tweezers to estimate the force produced by moving vesicles in the giant amoeba *Reticulomyxa* spp. (12). The laboratories of K Greulich and M Berns have combined cw infrared optical tweezers with either pulsed ultraviolet or pulsed Nd:YAG laser microbeams, which function as optical scalpels, to cut and paste. With this arrangement, they performed various kinds of microsurgery, such as laser-assisted cell fusion (76). Greulich's group has employed optical scalpels to sever isolated chromosomes and optical tweezers to collect the pieces for eventual use in gene sequencing procedures (45, 71). They have also initiated studies bringing together killer T-cells and target cells with

optical tweezers for studies of the immune response (71). Berns and colleagues have manipulated chromosomes or chromosome fragments in order to study cell division (19, 21, 56, 57, 85), and Aufderheide has repositioned micronuclei and small organelles in *Paramecium* spp. (13, 14). Much interest has focused on measuring the swimming force of sperm, and optical methods may potentially facilitate in vitro fertilization (36, 79). Optical tweezers can be used to separate individual cells out of a mixed culture, for example bacteria (11) or yeasts (47). In fact, a prototype sorter for eukaryotic cells has been built based on optical forces (28, 29), and a commercial version of optical tweezers has been developed that is well suited to sorting and picking operations (LaserTweezers® 1000, Cell Robotics, Inc., Albuquerque, NM). By calibrating the optical force against viscous drag, Block, Blair & Berg (24) measured the torsional compliance of bacterial flagella. This compliance mainly resulted from the hook, a flexible helical polymer consisting of ~150 polypeptides that connects the shaft of the bacterial rotary motor to the filament (25). Charon et al used optical tweezers, in combination with video-enhanced differential interference contrast (DIC) microscopy, to immobilize spirochete bacteria and establish that their periplasmic flagella rotate (32).

One especially powerful approach has been the use of materials strongly trapped by optical tweezers, such as polystyrene or silica microspheres, as tiny handles. Handles can be more refractile than biological material, supplying extra trapping force, and their shape and uniform size facilitate calibration. Chu and coworkers attached polystyrene spheres to one or more ends of single molecules of DNA, which can be visualized in fluorescence using intercalating dyes. Using this approach, they initiated studies of mechanical properties by stretching a molecule taught, then releasing one of its ends and following the relaxation to a random coil (33). Shepherd et al attached myosin molecules covalently to polystyrene spheres, then captured such spheres out of suspension using optical tweezers and deposited them directly onto actin cables derived from demembranated hair cell stereocilia (72). In the presence of ATP, the myosin molecules pulled the spheres unidirectionally along the length of the actin, providing a novel in vitro motility assay for myosin. Silica spheres coated with the motor protein kinesin were similarly captured and placed on axonemes or microtubules in the presence of ATP, whereupon they moved unidirectionally (26).

The use of optical tweezers improves the efficiency of in vitro moving-bead assays by several orders of magnitude, permitting one to work at such dilute concentrations of kinesin protein that beads carry just

one motor molecule (26). Using an in vitro assay, Kuo & Sheetz (55) estimated the force produced by molecules of kinesin. Edidin et al (40) and Kucik et al (53) used particles attached to transmembrane proteins to monitor the motility in the plane of the membrane of these complexes in order to study diffusion and cytoskeletal transport. Svoboda et al (77) attached spherical handles to ghosts of human red blood cells and levitated such ghosts away from microscope chamber surfaces. The microscope chamber was then perfused with neutral detergents that dissolved the lipid membrane of the ghost, revealing the labile spectrin cytoskeleton and permitting study of its properties in the absence of complicating surface interactions. Kuo and colleagues (54) attached spherical handles to the outsides of cells and used optical tweezers to draw such particles away from the surface, pulling the membrane out into slender filaments resembling filapodia, which they dubbed "neopodia." Neopodia may provide a useful system for studying the dynamic reorganization of cytoskeletal elements in cells.

Recently, Svoboda et al (78) used beads carrying single molecules of kinesin to detect the tiny steps made by this mechanoenzyme as it moves along the microtubule substrate: this was accomplished by combining optical trapping with interferometric position detection. In related work, Simmons et al (75) are using a sophisticated double-trap arrangement, equipped with position detection and force feedback, for experiments to measure displacements and forces produced by single myosin molecules interacting with actin filaments stretched between handles. A later section of this review explores other uses of handles.

DESIGN CONSIDERATIONS

Building a Trap

Optical tweezers can be built into a conventional light microscope in several ways (22). Fundamentally, two rules must be observed. First, a single-mode laser beam should be introduced into the microscope in such a way as not to interfere with normal microscope function and brought to a tight focus at (or near) the specimen plane using an objective of high NA, typically ≥ 1.00. Arranging the optics so that the trap is parfocal with the specimen allows trapped objects to be visualized and improves the quality of the trap, because microscope optics are designed to minimize aberrations near the specimen plane. A high NA is essential to maximize the light gradient near the focal region and thereby to ensure stable trapping in the axial direction. Second, the effective diameter of the laser beam (usually taken to be the $1/e^2$ di-

ameter of the Gaussian beam) should be adjusted to exactly fill, or somewhat overfill, the back pupil of the objective. Most often, this is accomplished by placing a laser beam expander (or some other lens pair) in the optical system before the light enters the microscope, but one can also use the natural laser beam divergence in combination with a longer beam path. Filling the back aperture of the objective assures that light converges to a tight, diffraction-limited spot.

Practical optical traps implement additional features, such as some means of shuttering or switching the laser to turn the trap on and off. A variable light level is also desirable. Laser attenuators may be built around neutral density filters or wedges, or, for polarized lasers, around variable-extinction devices (e.g. a rotating half waveplate in combination with a fixed polarizer), or acousto-optic modulators. The power in certain lasers, especially diode and diode-pumped lasers, may be readily altered by adjusting the operating current.

Often, the trap must be moved with respect to the specimen, which can be done either by moving the specimen or by moving the beam. In practice, both capabilities are helpful. Specimens can be positioned in the x-y plane by moving the microscope stage in the conventional way while leaving the trap fixed on the optic axis. This is especially useful when large-scale movements are required, i.e. over distances greater than the microscope field of view. A computerized, motorized stage can be used to automate movement, as in one commercial instrument (LaserTweezers® 1000, Cell Robotics). For small but accurate displacements, the sample may be mounted on an x-y piezoelectric stage. Movement of the trap in depth (the z-direction) is accomplished by focusing the microscope up or down (a process that also may be motorized), taking advantage of the parfocality of trap and specimen. Alternatively, the sample—or the objective, for that matter—can be placed on a vertical piezoelectric element. The trap can be displaced vertically with respect to the specimen plane by changing the parfocalizing optics, most often by moving an external lens controlling beam divergence.

Beam Steering

For rapid and convenient movement within the field, the trap may be steered in the specimen plane. To accomplish this, the laser beam must be scanned over the specimen while maintaining illumination across the full back aperture of the objective. This is essentially the same problem solved by laser scanning confocal microscopes, and solutions developed for those devices are readily adapted to optical tweezers.

Figure 2 shows four different schemes used for beam steering with

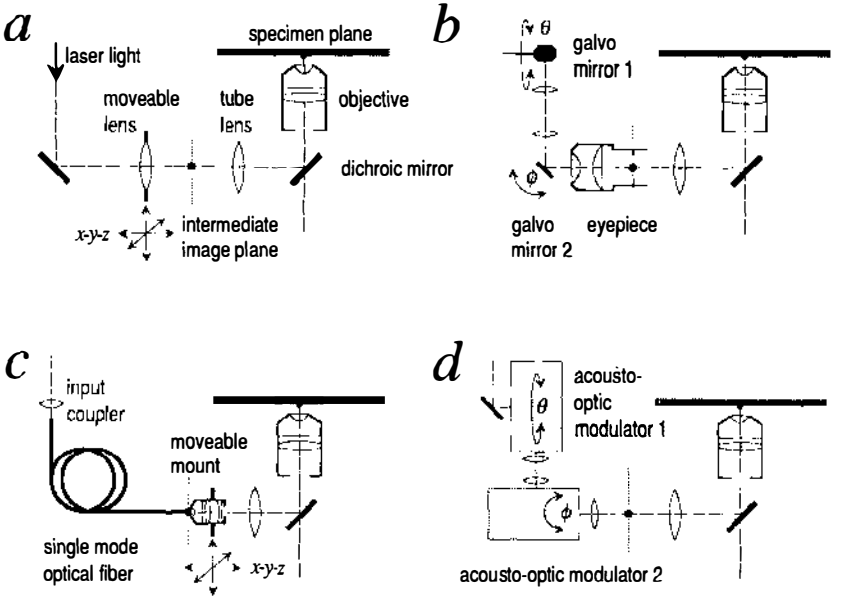

Figure 2 Four ways to scan the position of an optical trap in the specimen plane (see text). (*a*) Translating a moveable lens. (*b*) Rotating galvanometer mirrors. (*c*) Translating the end of an optical fiber. (*d*) Deflecting the beam with acousto-optic modulators (AOMs).

optical tweezers; objective lenses are drawn, for simplicity, with their rear focal plane at infinity. Figure 2*a* depicts an arrangement that is perhaps the most straightforward to build, in which the rear element of a two-lens telescope is moved by an *x*-*y*-*z* positioner (22). The front lens of the telescope may be the tube lens of the microscope that forms the intermediate image, or it may be some other lens external to the microscope light path. Translations of the rear lens in all three dimensions generate, to a good approximation, corresponding translations of the laser trap. This optical arrangement does not strictly produce the required rotation of the laser beam in the rear pupil of the objective, but it approximates that motion for small displacements, roughly within the center third of the field of view. Because it is mechanical and involves moving a relatively massive lens, it is slow, although scan rates to 100 Hz are still feasible (24). The scheme is simple, economical, lowest in terms of light loss, and quite stable (no drift), which may be vital to some specialized applications. It can be motorized and/or automated, if desired. It also provides for *z*-motion of the trap, in effect combining scanning and parfocality functions.

The scheme in Figure 2*b* is adapted directly from scanning confocal usage. Rotations of the galvanometer mirrors in θ and ϕ, which are placed in planes conjugate to the rear pupil of the objective, scan the beam in x and y. The first mirror is placed at the eyepoint of an eyepiece (or some other scan lens) that has been focused on the specimen. The 1:1 telescope lens pair between the galvanometer mirrors serves to image one mirror onto the other, so that they lie in conjugate planes, as well as to parfocalize the trap and image. An alternative is to place a single mirror at the eyepoint that can swivel in both θ and ϕ, driven through gimbal arrangement consisting of two nested galvanometers (not shown). The latter arrangement is somewhat slower, since one galvanometer must turn another one instead of just a lightweight mirror, but it may suffer less light loss. Although they are more costly and difficult to build, galvanometer-based scanners have a clear advantage of speed (rates up to several kilohertz), and they can scan the entire field of the microscope with minimal aberration. Moreover, they can be used to create multiple traps (84) and even different effective trap shapes (68). Most galvanometer mirrors are subject to small amounts of pointing jitter (5–100 μrad, p-p) that make their use problematic when absolute stability is required.

The scheme in Figure 2*c* is in many respects similar to that in 2*a*, except that the light is supplied by a single-mode optical fiber, the output of which is positioned at an intermediate image plane. An optical lever consisting of the lens arrangement shown moves the light-source position, which is steered mechanically with an x-y-z positioner (35). Optical fibers provide a convenient means of introducing laser light into an optical system.

The scheme in Figure 2*d* is similar to that in 2*b*, except that galvanometer mirrors are replaced by proportional acousto-optic modulators (AOMs). Such devices are quite expensive, relatively lossy (<85% transmittance per device), introduce aberrations, and are only capable of moderate deflections. However, they are unmatched for speed—frequencies approaching GHz are possible—and they have improved pointing stability over galvanometer mirrors. AOMs are best suited to specialized applications, such as force-feedback control.

The greatest light loss in optical trapping microscopes is sustained in the objective itself. Microscope manufacturers don't generally design lenses for transmittance in the near infrared, and as a result, antireflective coatings optimized for the visible spectrum can attenuate trapping lasers severely. The many optical surfaces present in compound lenses—up to 20 or more in the better objectives—do nothing to improve throughput. Numbers vary considerably, but in practice,

one can only expect to get about half of the incident light through an objective of high numerical aperture, as shown in Table 1. Considerable care should be taken when measuring the transmittance of microscope objectives: the large divergence of light from the focus prevents one from simply placing a photodector behind the specimen position and getting a reliable measure of throughput. A better method is to use an optical bench to align two identical objectives facing one another on either side of a symmetric specimen (two coverglasses with immersion medium, with a water layer in the middle), and pass collimated laser light through the pair, in such as way as to fill the pupil of each objective. Measuring the light transmitted by such a pair circumvents the problems arising from divergence and provides a realistic simulation of the configuration actually used for trapping. Unfortunately, it requires two matched objectives. The transmittance data of Table 1 were acquired by this method; these do not take into account any additional losses sustained at the back aperture.

Trapping Lasers

To prevent damage by light absorption, most trapping lasers operate in the near infrared, where a window of transparency for biological material arises from two opposing trends (Figure 3). First, natural biological chromophores, such as hemoglobin (Figure 3) or the ubiquitous cytochromes, absorb increasingly less light towards the near infrared, dropping out beyond wavelengths of ~800 nm. Second, water absorption rises dramatically as one goes farther into the infrared, peaking around 3 μm. An obvious compromise is the Nd:YAG laser at 1064 nm (or equivalently, the newer Nd:YLF laser at 1047 or 1053 nm), which is capable of the relatively high powers needed for trapping. Recently, single mode infrared diode lasers of sufficient power and beam quality

Table 1 Objective transmittances in the near infrared

Manufacturer	Type designation	Part number	Magnification	Numerical aperture	Transmittance at 1064 nm (±2%)
Carl Zeiss, Inc.	Plan Neofluar	44 04 80	100×	1.30 oil	59%
Carl Zeiss, Inc.	Plan Neofluar	44 04 66	63×	1.25 oil, iris	60%
Carl Zeiss, Inc.	Plan Apochromat	44 07 60	63×	1.40 oil	49%
Carl Zeiss, Inc.	Achrostigmat	44 02 55	40×	1.30 oil	49%
Nikon, Inc.	CF Fluor	85005	100×	1.30 oil	68%
Nikon, Inc.	CFN Plan Apochromat	85020	60×	1.40 oil	42%
Nikon, Inc.	CF Fluor	85004	40×	1.30 oil	74%

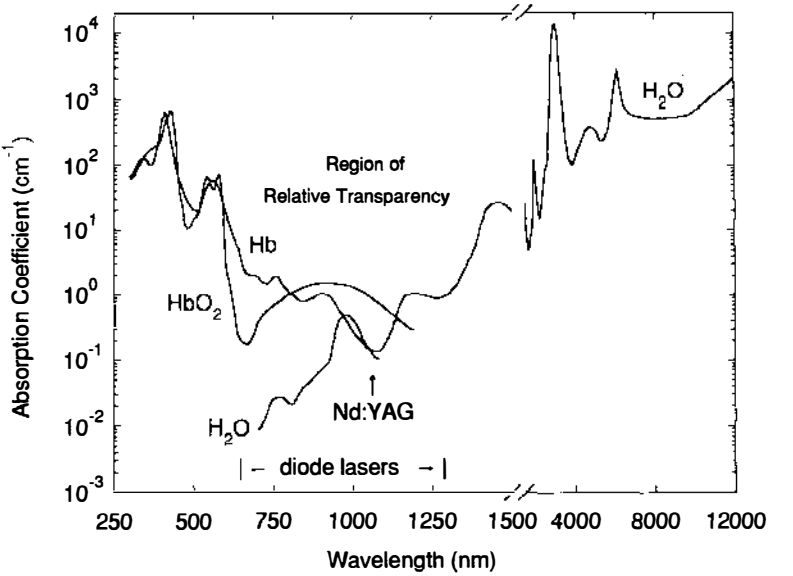

Figure 3 A graph illustrating the relative transparency of biological material in the near infrared region, showing the absorption of water and some common chromophores as a function of wavelength. Hb and HbO_2 stand for deoxyhemoglobin and oxyhemoglobin, respectively (at concentrations of 2×10^{-3} M). Water absorbs strongly beyond 2 μm. The wavelengths for Nd:YAG and diode lasers are indicated. Note the break in scale.

for trapping became available, and improved versions can be expected in the near future. Powers up to 1 W are now available commercially. Infrared diode lasers emit in narrow wavebands from ~780 to 1330 nm, with 820-860 nm being typical for trapping use. The tunable, externally pumped titanium sapphire laser can be varied continuously over the range of ~700–1100 nm. Table 2 serves as a comparative guide to lasers suitable for optical trapping.

Early work suggested that longer-term exposure to light at 1064 nm from a Nd:YAG laser produced photodynamic damage to cells, probably by optically pumping singlet molecular oxygen, a toxic free radical (22). Berns and colleagues have begun an important study of optical damage as a function of wavelength in the near infrared region using the tunable titanium sapphire laser, assaying chromosomal damage to mitotic cells (85). They covered the region from 700–840 nm, or roughly half the span of wavelengths available to this laser. Over this limited range, cells appeared minimally sensitive to irradiation around 700 nm and around 820 nm, but maximally sensitive at an intermediate value around 760 nm. The lower damage at 820 nm augurs well for the use

Table 2 Near infrared optical trapping lasers

Laser type	Gain medium	Wavelength (nm)	Power min–max (typical)	Some suppliers	Price range (1993, *approximately*)	Remarks
Conventional solid state (TEM_{00} mode, cw)	Nd:YAG, Nd:YLF	1064, 1320 1047, 1053	0.5–20 W (1 W)	Coherent, CVI, Lee, Quantronix, Spectra-Physics, Spectron	$5,000–40,000	Most power; some alignment required; less stable; cooling water system required; least expensive for high power
Tunable solid-state (TEM_{00} mode, cw)	Ti:Sapphire	~700–1100, variable	150 mW–3 W (1 W)	Coherent, E-O Schwartz, Spectra-Physics	$20,000–40,000	Tunable, power varies with wavelength; alignment required; less stable; requires multiwatt argon or Nd:YAG laser pump source and cooling system; most expensive
Diode-pumped solid state (TEM_{00} mode, cw)	Nd:YAG, Nd:YLF	1064, 1320 1047, 1053	100 mW–4 W (300 mW)	Adlas, Amoco, Coherent, Laser Diode, Spectra-Physics	$10,000–40,000	Moderate power; turnkey operation, no alignment required; stable; usually thermoelectrically (TE) cooled; moderately expensive
Laser diode (single mode, cw)	GaAlAs, InGaAs, InGaAsP	780–1330 (850 typical)	40–250 mW (100 mW)	EG&G, Liconix, Melles Griot, Oki, Sharp, Sony, Spectra Diode Labs, Toshiba	$200–3000 (not including power supply, beam optics)	Lower power only; stable; beam circularization optics required; separate power supply required; TE cooling optional; nearly diffraction-limited; least expensive
Hybrid laser diode (single mode, cw) master oscillator power amplifier (MOPA)	InGaAs	985	1 W	Spectra Diode Labs	$10,000 (not including power supplies)	Highest power for single diode; stable; onboard TE cooler and beam circularization optics; three external power supplies required; nearly diffraction limited; relatively expensive

of diode lasers, which are convenient, economical, and available at this wavelength. Because minimal damage occurred at the extrema of the range, the wavelength spread needs to be extended in future study. Studying optical damage to biological systems on a case-by-case basis may also become necessary, since the mechanisms of photodamage are not well established. The situation is complex: damage most likely does not arise from heating, per se (22), but several types of deleterious photochemistry may be operating. Some toxicity may also arise from two-photon effects, which occur even with cw lasers at the high fluxes encountered near the trapping zone (80). The threshold for optical damage, or *opticution* (a colorful term due to Ashkin), sets the practical limit on the amount of light that can be delivered, and therefore on the optical force that can be usefully provided. Clearly, these limitations need to be better defined.

TRAPPING THEORY

Optical forces are sensitive to small perturbations in geometry, and therefore theoretical computation will probably never replace direct measurement. But theoretical models are nevertheless useful to suggest improvements in experimental geometry and choice of trapping materials. Comparisons between experiments and models may also reveal the presence of other forces. One possibility is the radiometric force, generated by thermal gradients resulting from residual absorption by the trapped particle (6). To date, force calculations have dealt only with spherical dielectrics, primarily because electromagnetic models for other geometries are harder to compute. Also, polystyrene and silica handles are spherical. Finally, any baseline lessons, parametric trends, and general wisdom can probably be transferred to the trapping of more complex specimens.

Optical forces are customarily defined by the relationship

$$F = \frac{Qn_{\mathrm{m}}P}{c}, \qquad 1.$$

where Q is a dimensionless efficiency, n_{m} is the index of refraction of the suspending medium, c is the speed of light, and P is the incident laser power, measured at the specimen (4). Q represents the fraction of power utilized to exert force. For plane waves incident on a perfectly absorbing particle, $Q = 1$. To achieve stable trapping, the radiation pressure must create a stable, three-dimensional equilibrium. Because biological specimens are usually contained in aqueous medium, the

dependence of F on n_m can rarely be exploited to achieve higher trapping forces. Increasing the laser power is possible, but only over a limited range due to the possibility of optical damage. Q itself is therefore the main determinant of trapping force. It depends upon the NA, laser wavelength, light polarization state, laser mode structure, relative index of refraction, and geometry of the particle.

In the Rayleigh regime, trapping forces decompose naturally into two components. Since, in this limit, the electromagnetic field is uniform across the dielectric, particles can be treated as induced point dipoles. The scattering force is given by

$$\mathbf{F}_{scatt} = n_m \frac{\langle \mathbf{S} \rangle \sigma}{c}, \qquad 2.$$

where

$$\sigma = \frac{8}{3} \pi (kr)^4 r^2 \left(\frac{m^2 - 1}{m^2 + 2} \right)^2 \qquad 3.$$

is the scattering cross section of a Rayleigh sphere with radius r (52). $\langle \mathbf{S} \rangle$ is the time-averaged Poynting vector, n is the index of refraction of the particle, $m = n/n_m$ is the relative index, and $k = 2\pi n_m/\lambda$ is the wave number of the light. Scattering force is proportional to the energy flux and points along the direction of propagation of the incident light. The gradient force is the Lorentz force acting on the dipole induced by the light field. It is given by

$$\mathbf{F}_{grad} = \frac{\alpha}{2} \nabla \langle E^2 \rangle, \qquad 4.$$

where

$$\alpha = n_m^2 r^3 \left(\frac{m^2 - 1}{m^2 + 2} \right) \qquad 5.$$

is the polarizability of the particle (44). The gradient force is proportional and parallel to the gradient in energy density (for $m > 1$). Stable trapping requires that the gradient force in the $-\hat{z}$ direction, against the direction of incident light, be greater than the scattering force. Increasing the NA decreases the focal spot size and increases the gradient strength. Hence, in the Rayleigh regime, trapping forces in all directions increase with higher NA. For a trapped particle, the effect of $\mathbf{F}_{scatt}$ is to move the equilibrium trapping position down-beam from the laser focus. Although a decomposition into scattering and gradient

forces is not strictly meaningful for larger particles, the nomenclature is nevertheless retained (see section on ray optics, below).

Most theoretical models have been limited to either Rayleigh or Mie scatterers. In the Rayleigh regime, Visscher & Brakenhoff (82) computed the dependence of axial forces on NA and wavelength. They used a form of the incident beam based on vector diffraction theory (64), valid for uniform illumination at the back aperture of a high NA objective. Models for Mie scatterers (15, 47a, 83, 92) have been based on the formalism of Roosen (65, 66) for the computation of optical forces caused by reflection and refraction at a spherical surface, and have neglected diffraction effects. But some of these computations assume a TEM_{00} mode structure at the focus (15, 47a, 92) that is only valid for low NA systems, since for higher NAs the paraxial approximation breaks down (38, 73). In a more generally applicable theory developed by Visscher & Brakenhoff, a high NA beam structure was used to compute axial trapping forces as a function of NA and index of refraction (83). They used the Poynting vector at a point on the sphere's surface to define the phase and angle of incidence. Although this strategy is physically incorrect (4), it probably gives qualitatively correct results. They predicted a maximum trapping force for $n = 1.65$ (for $r = 15\ \mu$m, NA $= 1.3$, $\lambda = 1064$ nm), similar to the prediction of the ray-optics (RO) model described below. At this high index, however, the large scattering force will tend to accelerate particles in the neighborhood of the trap away from the focus and, in effect, make stable capture more difficult. Ashkin derived axial and trapping forces based on a simple RO model (4).

In the intermediate regime, where $r \leq \lambda \approx 1\ \mu$m, recent electromagnetic (EM) calculations employing a more rigorous approach to the boundary value problem appear to describe trapping forces better than the RO model (16–18, 90, 91). Because the RO theory is the most complete, but the size regime of the EM theory arguably the most relevant, we discuss these two approaches in more detail.

Ray-Optics Theory

Building on the work of Roosen, Ashkin (4) computed optical forces for the Mie regime ($r \gg \lambda$). A known distribution of parallel rays enters the back focal plane of an objective, which is assumed to focus all rays to a point. Diffraction effects are neglected in this limit, by definition. The rays both reflect and refract at the surface of the sphere, giving rise to optical forces. The force, **F**, due to a single ray of power, P, is given by

$$\mathbf{F} = \frac{n_m P}{c}\left\{1 + R\cos 2\theta - \frac{T^2[\sin(2\theta - 2\epsilon) + R\cos 2\theta]}{1 + R^2 + 2R\cos 2\epsilon}\right\}\hat{\mathbf{k}} + \frac{n_m P}{c}\left\{R\sin 2\theta - \frac{T^2[\sin(2\theta - 2\epsilon) + R\sin 2\theta]}{1 + R^2 + 2R\cos 2\epsilon}\right\}\hat{\mathbf{l}}, \quad 6.$$

where θ is the angle of incidence, ϵ is the angle of refraction, $\hat{\mathbf{k}}$ and $\hat{\mathbf{l}}$ are unit vectors parallel and perpendicular to the direction of the incident ray, and R and T are the Fresnel reflection and refraction coefficients (49). R and T are polarization dependent, and therefore so are the trapping forces. In Ashkin's notation, the coefficients of $\hat{\mathbf{k}}$ and $\hat{\mathbf{l}}$ represent the scattering and gradient forces, respectively. The force includes the effects of all internally reflected and refracted beams, hence, it is exact within the RO approximation. The overall force exerted by a beam with a given profile is simply the vector sum of the forces resulting from the ensemble of rays that comprise the beam. Figure 4 illustrates the basic geometry for ray-optic calculations.

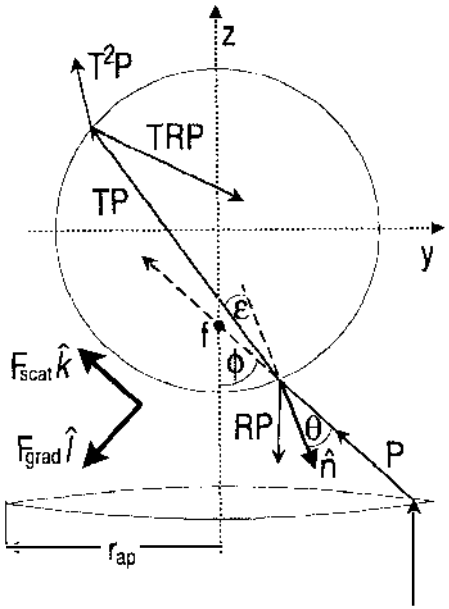

Figure 4 Ray-optics diagram of a single beam trap (after Ref. 4), shown with the objective below, as in an inverted microscope. The focus, f, is located on the *z*-axis. Variables: q, the angle of incidence for a ray; e, the angle of refraction; ϕ, the cone half-angle of the incident beam; $\hat{n}$, a surface normal; r_{ap}, the aperture radius. A single incident ray of power P gives rise to reflected and refracted rays of power RP, TP, T^2P, TRP, etc. Gray arrows indicate the directions of scattering and gradient forces. Note that the forces act through the center of the bead and do not exert torques.

In the RO regime, trapping forces are independent of sphere size, and the smallest forces occur in the $-\hat{z}$ direction. In this direction, the gradient force must overcome the axial scattering force. Therefore, the strongest trap is achieved by maximizing the restoring force in this direction, even at the expense of other force components. The RO theory predicts that *overfilling* the back pupil of the objective, i.e. $\omega_o > r_{ap}$, where ω_o is the beam radius of the TEM_{00} mode at the objective back aperture and r_{ap} is the lens aperture radius, leads to stronger trapping than simply filling the back pupil (4). This is because highly converging rays contribute disproportionately to the axial intensity gradient. The loss of laser power suffered by overfilling the back aperture is generally not a problem, because most trapping applications require only a few milliwatts at the specimen plane. For the same reason, objectives with the highest possible NA are most useful. In principle, laser mode profiles that concentrate a greater fraction of light at larger angles should do even better. Ashkin discusses use of the TEM_{01}^*, or donut mode, which has an intensity distribution of the form $I(r) = I_o(r/\omega_o)^2 \exp(-2r^2/\omega_o^2)$. Either overfilling the back aperture with the TEM_{00} mode or filling the back aperture with the TEM_{01}^* mode profile at NA = 1.3 should produce a ratio of forces in the strongest $(+z)$ and weakest $(-z)$ directions of 1.75–2.00. This ratio increases with decreasing axial gradients. In the $-z$ direction, the dependence of trapping forces on relative index of refraction should reach a maximum at $n = 1.69$. This observation implies that polystyrene particles ($n = 1.57$) should trap better than silica particles ($n = 1.47$). The decrease of trapping force at larger n (>1.69) results from a disproportionate increase in the scattering force. Theory predicts that the axial and transverse stiffnesses of the trap (i.e. dF/dz, dF/dy) increase towards the edge of the trapping zone.

One curious prediction of the RO model is that the transverse trapping efficiency should decrease with increasing NA (or decreasing focal spot size) over some range of NAs, i.e. that transverse forces vary nonmonotonically with transverse gradient fields. The fact that, under some circumstances, trapping due to the "gradient force" actually *decreases* with steeper gradients clearly shows that the simple decomposition into scattering and gradient forces breaks down outside the Rayleigh regime.

Electromagnetic Theory

Biological applications of optical tweezers often use spherical dielectric handles with diameters of 0.2–1.0 μm. For such particles, diffraction effects are significant. Moreover, for highly forcused beams, the vector

character of the electromagnetic field cannot be neglected, as is generally the case in scalar theories that use the paraxial approximation. These factors enormously increase the difficulty of computing realistic forces in the intermediate size regime. The time-averaged force due to an arbitrary electromagnetic field, acting on an arbitrary particle, is given by the following integral over the surface enclosing the particle:

$$F_i = \left\langle \oint_S \mathbf{T}_{ij} \mathbf{n}_j da \right\rangle, \qquad 7.$$

where $\mathbf{T}_{ij}$ is the Maxwell stress tensor, $\mathbf{n}_j$ is the outward unit normal vector, and the brackets denote a temporal average. The appropriate form of the stress tensor has been the subject of some controversy. The consensus appears to be that for steady-state fields, the Minkowski form (49),

$$\mathbf{T}_{ij} = \frac{1}{4\pi}\left[\epsilon E_i E_j + B_i B_j - \frac{1}{2}(\epsilon E_i E_i + B_i B_i)\delta_{ij}\right], \qquad 8.$$

where ϵ is the electric permittivity, is the correct one to use (18). The difficulty lies in deriving all six components of the electromagnetic field, E_i and B_i, at the surface of the particle, because the field includes contributions from the incident beam as well as the scattered and internal fields.

For incident light, the electromagnetic vector potential can be expanded in powers of the beam parameter, $s = \lambda/2\pi n_m \omega_o$, where λ is the wavelength and ω_o is the beam waist (38). The usual paraxial treatment for Gaussian laser beams is equivalent to a zeroth order approximation, i.e. it is valid for $\omega_o \gg \lambda$. Clearly, for highly focused beams, $\omega_o \leq \lambda$, this approximation is invalid. Even qualitative information gained by zeroth-order computations with Gaussian beams should be viewed with suspicion, because all axial fields are first order in s. Barton et al have derived all six electromagnetic field components in the focal region using a fifth-order correction to the paraxial Gaussian beam approximation (16). Their improved approximation is valid in the focal region of high NA objectives (within a 0.5-μm radius) illuminated by TEM_{00} mode beams.

In related work, Barton and coworkers derived a theoretical framework to compute scattered and internal fields for a sphere illuminated by an arbitrary monochromatic wave (17). The force follows from knowledge of the field at the surface of the sphere and Equations 7 and 8. For example, they derived the radiation force and torque on a 5-μm-diameter water droplet (18). These calculations were in quali-

tative agreement with experiments in which polystyrene particles and glycerol droplets were levitated with focused laser beams (5).

Recently, Wright and coworkers (90) used EM theory and RO theory to compute the maximal axial trapping efficiency, Q_{max}, for polystyrene particles ($n = 1.57$), as a function of particle size (Figure 5). For small radii ($r < 0.1$ μm), trapping force scales with r^3, as expected for Rayleigh scatterers (Equation 5). The largest Q_{max} is predicted to be 0.14, corresponding to forces of 4.4 pN/mW. Their experimental measurements of Q_{max} for 1-μm-diameter silica spheres and 10-μm-diameter polystyrene spheres showed that EM theory gives better estimates for $r < 1$ μm than RO theory, and that RO theory gives acceptable results for $r > 10$ μm (at $\lambda = 1064$ nm). However, the discrepancy between EM theory and experiment for the 1-μm particle is still a factor of 3–5 depending upon the actual value used for objective transmittance (WH Wright, personal communication). The RO theory does somewhat better, but in general, measured Q values are low compared with theory. The discrepancy between theory and measurement may result from radiometric forces, but this remains to be determined. In the range 1–10 μm, neither EM nor RO theories seem to produce accurate results. Even a ninth-order correction does not help to prevent the breakdown of the EM theory for particles larger than 1 μm or the breakdown of the fifth-order Gaussian beam approximation far from

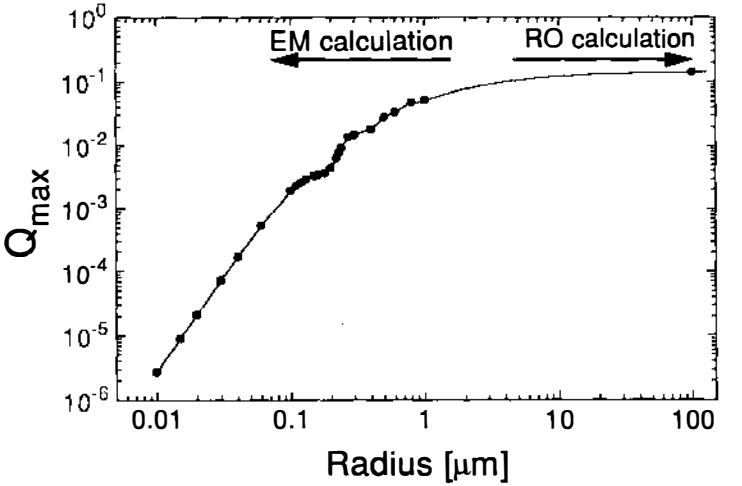

Figure 5 Computed maximum axial trapping efficiency (Q_{max}) as a function of sphere radius (redrawn from Ref. 90). Parameters were $n = 1.57$, $n_m = 1.33$, $\lambda = 1064$ nm. For the EM calculation, the spot size was 0.4 μm. For the RO calculation, the maximal cone half-angle was 60°.

the focus (WH Wright, personal communication). Wright et al also computed the axial trapping efficiency as a function of the distance between the sphere and the focus for a 1-μm-diameter silica sphere (90). In contrast to RO theory, the axial stiffness is predicted to decrease towards the edge of the trap. This behavior is in general agreement with our own measurements on 0.6-μm silica beads (see Figure 10*a* in the section on picotensiometers, below).

Although considerable work has gone into predicting optical forces, the agreement between theory and measurement is unsatisfactory; whether the quality of the measurements or of the models is responsible is unclear. Future force calibrations should be done with great care and combined with measurements of the beam profile at the focal plane, for comparison with theory (70, 91). The power actually delivered to the specimen ought to be reported, not merely the incident power to the system. Possibly, the microroughness of particle surfaces, a physical property not considered in any of these models, might contribute to scattering force (60). Finally, radiometric forces may play some role.

Parametric trends predicted by the EM and RO models have not been rigorously tested. One obvious candidate is the dependence of the axial trapping efficiency, Q_{max}, on particle radius. Another is the dependence of Q_{max} on the spot size and beam profile (91). It may be possible to apply self-consistent lattice models, in which the dielectric is represented as a collection of point dipoles on a lattice, to improve modeling. This approach has been successful in computing scattering by nonspherical objects (62).

FORCE MEASUREMENT

Calibration

Because current theory is unreliable in the computation of trapping force for particular objects and trapping geometries, these forces must be determined empirically. In most applications, forces are calibrated against viscous drag exerted by fluid flow. Calibration is facilitated by the fact that the Reynolds number is typically quite small for micron-sized objects: $Re = va\rho/\eta \approx 10^{-5}$, where v is the fluid velocity, a is the particle size, ρ is the particle density, and η is the fluid viscosity. Inertial forces are therefore entirely negligible, and the drag force on a stationary object if $F = \beta v$, where β is the drag coefficient and v is the fluid velocity (48). For a sphere of radius a, β is given by Stokes' Law: $\beta = 6\pi\eta a$. Drag forces on ellipsoids have also been derived in closed form (27, 48).

The maximal, or escape force, is typically measured in one of three ways (Figure 6):

1. Using a flow chamber, fluid is pumped past a stationary, trapped sphere at increasing velocity until the object just escapes (Figure 6*a*). The local fluid velocity is then measured by tracking the object immediately after leaving the trap, or by tracking some other object in the flow field in the same focal plane. This procedure requires only video microscopy and a flow chamber connected to a variable pump, but it has several drawbacks. First, since trapping is often done near a wall of the chamber, the shear field in the flow tends to push the trapped particle out of the focal plane towards the coverslip, and the force measured may differ from the actual force at the focal plane. Second, since only relatively slow particle velocities (~20 μm/s) can be measured with video methods, only small forces can be measured. Third, the method is confined to measuring transverse trapping forces.

2. The chamber containing fluid is moved past a stationary trapped sphere, and the velocity of the stage at which the bead escapes is measured (Figure 6*b*). In this case, a motorized or piezo-driven stage

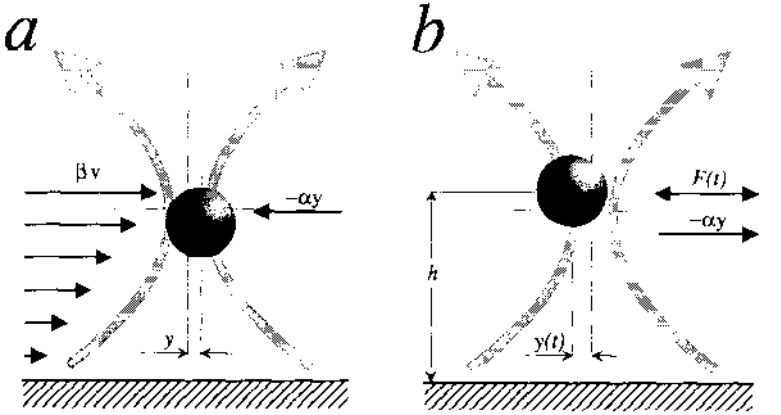

Figure 6 Schemes for force calibration. Laser light (*gray arrows* depict the sides of the beam profile) enters from below through a coverslip (*hatched*), as in an inverted microscope, and is focused to a narrow waist, whose center is marked by dashed lines. (*a*) The bead and chamber are held stationary while fluid is drawn past. The fluid drag force is balanced by the trapping force. Note that the shear field (*left arrows*) pushes the particle towards the coverglass. (*b*) The bead is held stationary while the chamber is moved, such that it experiences a force, $F(t)$. Note that the scattering force moves the axial equilibrium point down-beam from the center of the focus. Variables: h, the distance from coverglass surface; $y(t)$, the transverse position of the bead with respect to trap center; $F(t)$, the applied force on the bead (or, for thermal motion in a stationary chamber, the Langevin force); $-\alpha y(t)$, the transverse restoring force due to trap.

is needed. The main drawback to this method is that the drag must be corrected for the proximity to the coverglass surface, the effect of which can be large when the distance from the surface is comparable to the particle radius, as shown in Table 3. The viscous drag coefficient of a sphere with radius a whose center is a distance h from the surface is (48):

$$\beta = \frac{6\pi\eta a}{\left[1 - \frac{9}{16}(a/h) + \frac{1}{8}(a/h)^3 - \frac{45}{256}(a/h)^4 - \frac{1}{16}(a/h)^5\right]}. \quad 9.$$

3. The optical trap is moved while the sample fluid remains stationary, and the velocity at which the bead escapes is recorded. This method is essentially equivalent to method 2 except that for some beam-steering configurations, notably those employing AOMs or galvanometer scan mirrors, larger velocities can be achieved and hence larger forces can be determined.

4. Axial trapping force can, in certain cases, be calibrated against gravity using an escape method. This approach is useful for particles that are sufficiently large and dense enough to have a negligible scale height, $h = kT/w$, where w is the net gravitational force acting on the object. The lower size limit is roughly 10 μm for polystyrene and 1 μm for silica particles. In principle, the gravity balance technique could

Table 3 Drag on a sphere near a planar surface (Faxen's Law)

(h/a)[a]	Drag relative to $h = \infty$
1.01	2.97
1.10	2.36
1.25	1.92
1.50	1.62
1.75	1.47
2	1.39
3	1.23
4	1.16
5	1.10
10	1.06
50	1.01
∞	1.00

[a] Variables: h, distance above surface of center of sphere; a, sphere radius. The drag on the sphere at $h = \infty$ is given by Stokes' Law, $\beta = 6\pi\eta a$.

be extended to measuring lateral trapping by turning the microscope on its side.

Several groups have determined transverse trapping forces by using these methods (11, 12, 25, 55, 69), but the interpretation of calibration measurements is not necessarily straightforward. For instance, Sato et al (69) noted that the axial equilibrium trapping position is a function of transverse position. This effect would lead to an underestimate of force in experiments that strictly confine the particle to the equilibrium plane. Ashkin's computations suggest that this underestimate leads to only a small error (~5%), at least for larger particles (4).

Calibration against gravity has been used to measure the axial Q_{max} for various objectives (91). The size of the focal spot, ω_o, for these objectives was also measured with a knife-edge scanning technique. For both 1-μm silica particles and 20-μm polystyrene particles, Q_{max} is a strong function of objective NA (and ω_o). Q_{max} ranged from 0.132 to 0.023 for NAs of 1.3 to 0.8 with 20-μm polystyrene particles. In the same study, Wright et al (91) found that Q_{max} decreased dramatically with distance from the coverslip surface, an anticipated effect, given the increase in spherical aberration with depth. Misawa et al (60) measured Q_{max} using a technique similar to method 2 by moving the stage vertically and measuring the escape velocity. Axial forces were on the order of 1–5 pN for 2- to 11-μm polystyrene particles (NA = 1.3, P = 43 mW).

Several investigators have verified the strict proportionality between transverse force and laser power (*cf* 24, 69). But for small forces and large particles, the gravitational force should alter the axial trapping position in a power-dependent fashion. At the lowest powers, therefore, the transverse trapping force should scale with power with an exponent somewhat greater than unity.

Measurement of Trap Stiffness

Most force measurements have been made using variations of the escape-force method just described. Convenience, sensitivity, and versatility, however, can be greatly enhanced if the force is instead determined as a function of displacement from the trap center, i.e. if the trap stiffness is found. To accomplish this, the position within the trap must be measured to nanometer or better resolution. One approach is to use a video-based centroid tracking method (42), but the limited dynamic range (~30 Hz) and spatial resolution (a few nanometers) present severe limitations. Nanometer resolution at kilohertz bandwidths can be achieved by imaging the object onto a split photodiode detector: the difference voltage is proportional to displacement for mo-

tions up to the order of the particle radius (50, 51). The detector must be aligned with the optical trap at all times. An alternative arrangement is to use an optical trapping interferometer, in which the same laser light serves to produce both the trapping and interferometer functions (78). Displacement is proportional to the ellipticity developed by polarized light after recombination of the interferometer beams. In this setup, the detector zone and the trap remain intrinsically aligned (see below).

Physics of Trap Stiffness Measurements

For a harmonic potential, the equation of motion of a trapped particle subject to thermal motion can be solved exactly. If y is the displacement of the bead from the trap center, β is the viscous drag, and α is the stiffness of the trap, then for low Reynolds number, the equation of motion is

$$\beta\dot{y} + \alpha y = F(t), \qquad 10.$$

where $F(t)$ is an external driving force (Figure 6*b*). In the simplest case, $F(t)$ is the Langevin (thermal) force. The resulting dynamics is that of Brownian motion in a parabolic potential well, characterized by a Lorentzian power spectrum (86):

$$S_{yy}(f) = \frac{kT}{2\pi^3\beta(f_0^2 + f^2)}. \qquad 11.$$

The corner frequency is $f_0 = \alpha(2\pi\beta)^{-1}$, and the mean square displacement of the particle is

$$\langle y^2 \rangle = 2\pi \int_0^{+\infty} S_{yy}(f)df. \qquad 12.$$

By the Equipartition Theorem, the mean square displacement is also equal to

$$\langle y^2 \rangle = kT\alpha^{-1}. \qquad 13.$$

These relationships suggest two ways to determine α by analysis of thermal fluctuations, both with inherent advantages. First, when the viscous drag is computable, e.g. for a spherical particle of known diameter located a known distance from the coverglass surface, the corner frequency, f_0, derived from a Lorentzian fit to the spectrum, gives a robust estimate of trap stiffness. A feature of this method is that the position detector itself need not be absolutely calibrated, because its calibration factor does not affect the corner frequency. Second, using a fully calibrated position detector, the mean square displacement,

computed by integration of the power spectrum (Equation 13), provides a measure of the stiffness that is independent of drag force. Since the stiffness computed in this way scales with the second power of the calibration factor, a well-calibrated position detector is essential.

The foregoing discussion assumes that trapping stiffness is constant during thermal fluctuations, i.e. that the potential well is parabolic. This is clearly an approximation valid for small amplitudes. However, one may wish to map the optical force profile at larger displacements. One convenient method is to move the fluid chamber with a sinusoidal motion at frequency f and amplitude x_0 while holding the trap fixed. The force on the bead is then $F(t) = 2\pi i f \beta x_0 \exp(-2\pi i f t)$. Solving Equation 3 for this driving force gives the trajectory

$$y(t) = \frac{x_0 f}{\sqrt{f_0^2 + f^2}} \exp[-i(2\pi f t - \delta)], \qquad 14.$$

where the phase shift is $\delta = -\tan^{-1}(f_0/f)$. Both amplitude and phase shift can be used to determine f_0 and thereby the trapping stiffness. One particularly useful limit is $f/f_0 \ll 1$, where the amplitude becomes

$$|y(t)| = x_0 f/f_0. \qquad 15.$$

At a fixed driving level, the amplitude of motion can be measured as a function of frequency. This relationship provides a direct measure of the linearity in the trap force profile: deviations from linearity at a given amplitude imply that anharmonic contributions to the potential enter in at this level. Results of a typical force calibration using this method are shown in Figure 10 of the section on picotensiometers, below. Similarly, triangular waveforms can be used to map out the force profile (55).

Brownian Motion During Force Measurements

Microscopic objects in a viscous medium display significant Brownian motion, thereby introducing noise into all force measurements. One can measure an external force, $Q(t)$, which has a power spectral density $S_Q(f)$, by observing the motion of a single bead (Figure 3*b*) in the presence of a Langevin force $L(t)$, which has a white power spectral density $S_L(f) = 2kT\beta/\pi$. The equation of motion of the bead is given by Equation 10, setting $F(t) = Q(t) + L(t)$. The power spectrum of bead motion becomes

$$S_y(f) = \frac{S_Q(f) + S_L(f)}{\alpha^2(1 + \gamma^2)}, \qquad 16.$$

where $\gamma = f/f_0$, and the two terms in the numerator come from the signal and noise, respectively (61a). The signal-to-noise ratio (*SNR*) for this situation can then be expressed as

$$SNR = \left[\frac{\int_0^{f_b} S_Q(f)/(1 + \gamma^2)\, df}{(2kT\beta/\pi) \int_0^{f_b} 1/(1 + \gamma^2)\, df} \right]^{1/2}, \qquad 17.$$

where the upper limit of integration, f_b, is the measurement bandwidth. How does the *SNR* vary with the trap stiffness, α? In general, the *SNR* will depend on f_b and the exact shape of $S_Q(f)$, but two particular cases are of special interest. For a slowly varying external force—as is usually the case when calibrating traps or measuring forces exerted by mechanoenzymes—$S_Q(f)$ rolls off at a frequency $f_Q \ll f_0$. Here, it is experimentally advantageous to choose a lowpass filter frequency for force measurements such that $f_b \geq f_Q$. When this is done, $\gamma \ll 1$ and Equation 17 reduces to

$$SNR = \left[\pi/2kT\beta f_b \int_0^{f_b} S_Q(f)\, df \right]^{1/2},$$

a result that is independent of the trap stiffness. Another special case occurs for a white signal, where $S_Q(f) = S_Q(0) = constant$ out to some frequency $f \gg f_0$. Equation 17 reduces to $SNR = (\pi S_Q(0)/2kT)^{1/2}$, once more independent of α. These two cases show that trapping force measurements, when appropriately filtered to maximize the *SNR*, can be made independent of the trap stiffness and need not be inversely proportional to the square root of that stiffness (75).

Picotensiometers

Several force transducers/tensiometers based on optical tweezers were recently constructed. For over 25 years, studies in physiology have focused on measuring the forces produced by muscle fibers. Analogous studies are now under way using modern in vitro motility assays, in which the action of just a few motor molecules at a time can be probed. In one such assay, myosin molecules are immobilized on a coverglass surface while actin filaments attached to silica beads are manipulated. For this work, S Chu, R Simmons, and J Spudich collaborated to develop a force transducer capable of exerting isometric tensions in the piconewton range over a bandwidth of several kilohertz (Figure 7). In

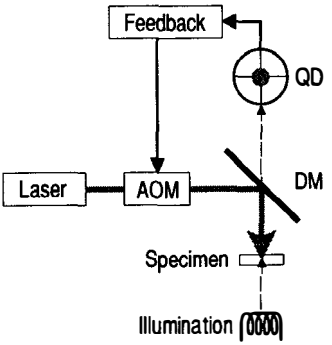

Figure 7 Simplified schematic of an isometric force transducer based on optical tweezers (after Ref. 75). QD, quadrant detector with bead image cast upon it; AOM, acousto-optic modulator(s); DM, dichroic mirror. The output of the quadrant detector is used to generate a feedback error signal that deflects the trap in such a way as to prevent the specimen from moving, i.e. to achieve the isometric condition: this error signal is proportional to the force produced by the object.

their scheme, the trapped bead is imaged onto a quadrant detector, the output of which is fed back to an acousto-optic modulator operating in deflection mode. The feedback signal is used to servo the trap rapidly to counteract the force fluctuations, Brownian and otherwise, of the bead. This effectively stiffens the trap. The record of the feedback signal supplied provides a measure of the force required to keep the bead stationary. Using this arrangement, these workers plan to measure the forces produced by small numbers of myosin molecules (75).

Svoboda et al (78) have developed an optical trapping interferometer (OTI) to measure the displacement of kinesin at subnanometer resolution while applying calibrated loads (Figure 8). In these assays, single kinesin molecules attached to silica beads are deposited by an optical trap onto microtubules immobilized on a coverglass surface. The subsequent motion of the beads is monitored by interferometry (39). The OTI takes advantage of standard differential interference-contrast optics in a modified inverted microscope. Polarized laser light is coupled to a single-mode, polarization-preserving fiber to eliminate pointing fluctuations of the laser. The beam is then introduced into the microscope at a point just below the objective Wollaston prism. This prism splits the light into two beams with orthogonal polarization; these are focused by the objective to two overlapping, diffraction-limited spots in the specimen plane. They function together as a single optical trap. A phase object located asymmetrically in the region illuminated by the two spots produces a relative retardation between the two beams.

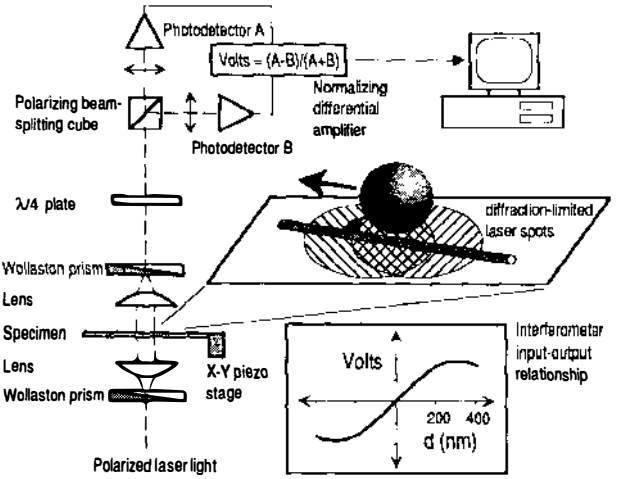

Figure 8 Schematic of an optical trapping interferometer, showing the optical components used for position detection (see text). (*Center*) A molecule of kinesin is shown pulling a bead along a microtubule in the direction shown by the arrow. (*Inset*) The output signal of this detector as a function of bead position.

When the beams interfere in the condenser Wollaston prism, elliptically polarized light results. The degree of this ellipticity provides a sensitive, nearly linear measure of displacement inside the trapping zone, in the direction of the Wollaston shear axis. A quarter waveplate, a polarizing beam–splitting cube, and a pair of photodiodes are used to measure the ellipticity. The normalized difference signal (V_{out}) carries the position information.

Detector noise is at or below 1 Å/Hz$^{1/2}$ (Figure 9). Since displacement information is encoded by the polarization of the laser light, this scheme is relatively insensitive to vibration, in contrast with imaging detectors, in which the position of the image with respect to the split photodiode carries the displacement information. Large laser light fluxes ensure that the detector does not become shot-noise limited at frequencies in excess of 100 kHz. The detector zone can be repositioned rapidly within the field of view of the microscope, because the same laser beam provides trapping and position sensing.

To calibrate the interferometer, a bead is immobilized on the coverslip surface and moved with a known waveform. The output voltage, V_{out}, is then measured as a function of displacement from the trap. This response function is approximately linear to ± 150 nm. Fitting a cubic polynomial to the response function allows one to determine the correspondence between V_{out} and displacement up to ± 200 nm from

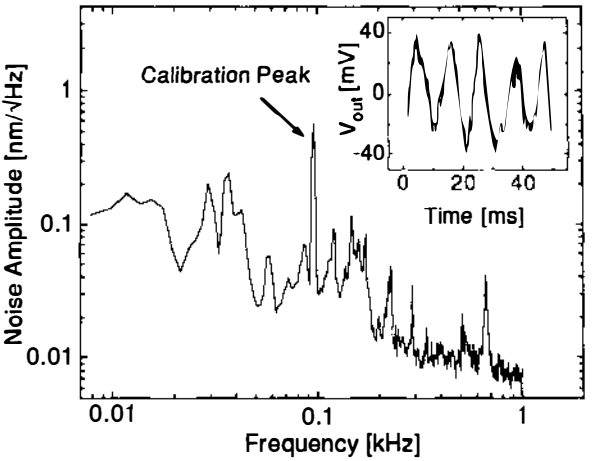

Figure 9 Sensitivity of the optical trapping interferometer. The graph shows the spectral noise density in response to a 100-Hz sinusoidal calibration signal of 1-nm amplitude. The large peak (*arrow*) corresponds to the signal; other peaks mainly result from acoustical interference and mechanical vibration. The raw detector output (*inset*) shows both the nanometer-sized signal and the noise, which is at the Ångstrom level.

the trap center to within a small error (~5%). Trap stiffness can be calibrated in any of the ways discussed above. Figure 10 shows the results of a typical force calibration.

Other Applications of Picotensiometry

Scanning force microscopy (SFM) has shown great potential for imaging nonconducting biological samples in solution at subnanometer resolution (63). In solid-supported Langmuir-Blodgett films, for example, single molecules can be imaged (41). However, on soft samples such as biological material, deformation caused by the heavy downbearing force [typically nanonewtons (89)] of the mechanical cantilevers used in typical SFM systems limits resolution and frequently damages the specimen irreversibly. This suggests the use of optically trapped objects as sensing elements for SFM. Compared with mechanical cantilevers, probe stiffness could be reduced by three to five orders of magnitude. Ghislain & Webb have used a tensiometer similar to the design shown in Figure 8 to scan an optically trapped stylus (a pointed glass shard, ~1 μm in length), over a nanofabricated test specimen (43). They placed a photodiode detector down-beam from the specimen, between optical planes conjugate to the specimen and to the objective back aperture. This photodiode serves as a sensor for the axial (z-) position. Since the transparent stylus acts like a small lens,

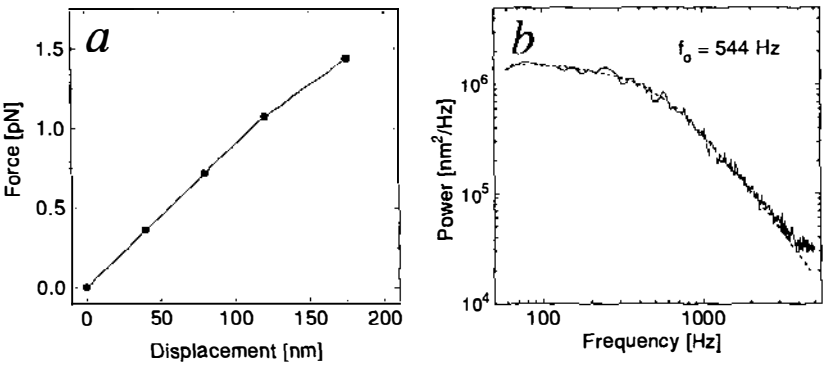

Figure 10 Force calibration of an optical trap. (*a*) Force versus displacement for a trapped silica bead (diameter ~0.6 μm; power ~14 mW), calibrated according to Equations 14 and 15 (x_o = 2 μm; β = 5.7 × 10^{-6} pN s/nm). Stiffness is constant out to 150 nm (α = 9.0 × 10^{-3} pN/nm), beyond which it decreases. (*b; Solid line*) The thermal noise spectrum of a trapped silica bead measured with the optical trapping interferometer (diameter ~0.6 μm; power ~28 mW). (*Dotted line*) The fit by a Lorentzian. The corner frequency of the Lorentzian (544 Hz) implies α = 1.9 × 10^{-2} pN/nm.

axial probe displacements with respect to the focus modulate the light intensity at the detector. To take a picture, the stylus is placed in contact with the surface using optical tweezers and scanned while its *z*-position is recorded. In this way, Ghislain & Webb detected topographical features with a lateral resolution of ~20 nm. Microfabricated tips should improve the resolution of this promising technique of optical force microscopy.

Determinants of Trapping Forces

Even for perfect dielectric spheres, trapping forces depend on several factors, and most of the parameter space remains unexplored, either theoretically or experimentally. For example, in our system, 0.6-μm silica particles are stably trapped as far as 200 μm from the coverglass surface, whereas for 0.52-μm polystyrene particles, the trap develops an axial instability just 10 μm from the surface. This difference illustrates the need to calibrate forces under conditions similar to those used in an experiment. Increasing any of the following parameters should improve the trapping force: numerical aperture of the objective (but possibly not in the RO regime), index of refraction of the trapped object (but only up to n = 1.69), laser power, particle size, and laser frequency. The following effects degrade trapping forces: small optical misalignments, increasing distance from the coverglass surface, non-optimal coverglass thickness, incorrect choice of refractive index for

the immersion oil, any additional sources of spherical aberration, back reflections and/or interference from scattered light, underfilling the objective back pupil, and laser beam wavefront distortion.

HANDLES

Biological macromolecules and macromolecular assemblies are often insufficiently refractile to be trapped alone with appreciable force. To facilitate trapping of such specimens, they are often attached to small refractile spheres, i.e. handles. One important consideration in handle attachment is surface chemistry. Unfortunately, no general principles seem to apply here. In certain cases, nonspecific attachment works quite well. For example, red blood cell cytoskeletons bind irreversibly to negatively charged silica bead surfaces, as do intact red blood cells and red cell ghosts (77). So, too, does native kinesin protein (26). Simple tricks sometimes produce favorable results: to attach handles to individual microtubules, we coated silica beads nonspecifically with avidin and bound these directly to biotinylated microtubules (R Stewart, K Svoboda & SM Block, unpublished data). Kuo & Sheetz (55) took a more elaborate approach, covalently linking bovine serum albumin (BSA) to carbodiimide-activated carboxylated polystyrene microspheres. The BSA was subsequently biotinylated and coated with avidin, and the avidin used to bind the beads to biotinylated microtubules. Actin filaments have been attached to silica beads by coating the beads with N-ethyl maleimide (NEM)-treated myosin or heavy meromyosin, which in turn binds tightly to actin (87).

Manufacturers (Polysciences, Bangs Laboratories, Seragen, Duke Scientific, etc) offer particles with a bewildering array of chemistries, including amine, carboxyl, and sulfate surface groups that facilitate coupling to proteins. Some form covalent linkages spontaneously using proprietary surface chemistry. Kits for attaching proteins to microspheres using antibody-based linkages or biotin-avidin are also available. Polystyrene beads come in a large assortment of sizes and colors, covering the useful size range for optical trapping (0.05–100 μm), and they are both round and homogeneous. Reasonably monodisperse silica beads in the 1-μm size range have only recently become commercially available (Bangs Laboratories). In the 0.5-μm size range, silica beads trap more readily than polystyrene. These advantages are partly offset by the relatively greater polydispersity in size and the smaller arsenal of surface chemistries of silica beads, which currently come with hydroxyl, amine, chloromethyl, or bromomethyl surface groups. How-

ever, several useful reagents are commerically available that chemically modify the surface of silica (Huls America).

The use of handles in biological applications of optical trapping will certainly continue to be important. In the future, aspherical designer handles, perhaps produced by microfabrication techniques, may provide substantially larger trapping efficiencies than spherical particles of the same volume, or may serve as better probes for the optical force microscope (above). The homogeneity, roundness, and size range of silica particles could be improved, as well as providing for larger variety of surface chemistries.

NOVEL TRAPPING GEOMETRIES

The use of optical tweezers for trapping is not without its disadvantages. Laser light must be focused to a tiny spot, generating enormous local fluxes (~5 MW/cm^2 for a 10-mW beam) and the possibility of optical damage. The size of the trapping zone is fixed and rather small, on the order of the light wavelength. The need for high NA objectives leads to short working distances and spherical aberrations that degrade trapping deeper into the sample chamber, away from the coverglass suface. In 1970, more than a decade before the single-beam gradient trap, Ashkin invented a stable optical trap based on two counter propagating beams that does not suffer from these problems. In this design, transverse trapping is supplied by the gradient force, but, in contrast to optical tweezers, the scattering force provides axial stability. Two counter propagating, coaxial beams with their waists separated by ~100 μm in the longitudinal direction form a stable equilibrium point, z_{eq}, for dielectric particles. Particles that encounter the beam on either side of this point are drawn towards the optical axis by the gradient force and simultaneously accelerated towards z_{eq} by the scattering force. Once there, the scattering forces in the two beams balance. For equal beam powers, z_{eq} is located at the geometrical symmetry point. Because the two trapping beams need only be weakly focused, this type of trap provides a long working distance, and it was used in a prototype device for automated cell separation (29). Unfortunately, the trap is comparatively difficult to implement with a conventional microscope, and its stability is critically dependent on the axial alignment of the two beams: for small misalignments, trapped objects move in tiny circular orbits around z_{eq}.

A simpler manifestation of this two-beam trap, based on optical fibers, was recently demonstrated (37). The counter propagating beams

are provided by two well-aligned, single-mode optical fibers, whose ends are placed opposite one another in the specimen plane and oriented perpendicular to the optical axis of the microscope. Because simple pigtail fibers coupled directly to diode lasers can be used and practically no additional optics are required, this design is perhaps the most economical optical trap of all (Figure 11). Strong forces transverse to the trapping beam axis (in the nanonewton range) can be achieved at relatively low power densities. The separation between the fiber ends (NA = 0.1) may be adjusted from 20 μm up to 280 μm and still capture particles from 0.1 to 10 μm in diameter, using laser power levels from 3 mW on up. One can alter the equilibrium position by reducing the power in one of the beams. A difficulty with this trapping arrangement is that the fibers must be aligned to within a micrometer or better, i.e. a fraction of the beam waist, to achieve stable trapping. Because stable fiber alignment in the current design depends on the mechanical support of the microscope slide, the trap is immobile in its present form. However, in principle this technical problem can be solved, and we can anticipate that a small trapping head will carry the fiber ends in alignment at some fixed separation and that this head can be moved throughout the microscope preparation on a conventional micromanipulator. Traps using counterpropagating beams should, in principle, be able to manipulate extremely high index particles (e.g. $n > 1.8$) that cannot be trapped by single beams owing to the loss of axial stability. With high index materials, still larger optical forces can be produced for a given laser power.

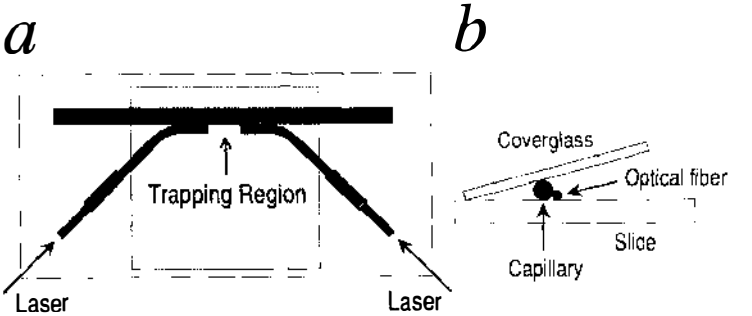

Figure 11 Schematic of the fiber-optic light force trap (after Ref. 37). (*a*) A 180-μm diameter glass capillary (*dark gray*) is sandwiched between a microscope slide (*white rectangle*) and a tilted coverglass (*light gray square*). Optical fibers (*black*) are channeled through two other short glass capillaries (*dark gray*) that are glued to the slide. The fibers are axially aligned by pressing them into the V-groove formed between the microscope slide and the capillary wall. (*b*) Side view, showing the V-groove.

Light-based radiation pressure has a direct acoustic analogue: both an acoustic scattering force and an acoustic gradient force are developed in interactions between matter and sound waves. Capitalizing on this analogy, Wu developed "acoustical tweezers" (93) based on a counterpropagating beam trap using 3.5 MHz ultrasonic transducers. A two-beam design was chosen to counteract the effect of acoustic streaming in the medium, which causes fluid to flow away from the transducers and would otherwise destabilize a single-beam trap. Thus far, the trap has been able to capture large (270-μm diameter) polystyrene spheres and clusters of frogs eggs. In principle, one could generate ultrasonic pressure waves with wavelengths smaller than those of visible light. However, acoustic lens technology lags far behind that of optical lenses, and it may prove difficult to focus acoustical waves to spot sizes smaller than those attainable with lasers. Nevertheless, acoustical tweezers may hold promise for several applications, particularly if they can be shown to produce significant forces without causing acoustic damage.

FUTURE DIRECTIONS

Prediction always carries an element of risk, but clearly optical forces stand poised to make important contributions to biological research. Light is a powerful tool. It can reach within sealed preparations—or even within living cells—to grasp and manipulate. Optical micromanipulators can work with double oil-immersion optics, affording the highest possible resolution in the light microscope. Displacements and forces produced by light can be controlled with extraordinary spatial and temporal precision. These properties bestow unique advantages upon optical force-based methods, as compared with conventional mechanical approaches.

Already, optical tweezers have been successfully used with a variety of different imaging techniques, including bright field (7, 11), phase contrast (21, 24), Nomarski DIC (22, 72), fluorescence (33, 75), and confocal microscopy (81). We anticipate that optical forces will eventually find applications in combination with microspectroscopy, light scattering, and perhaps even two-photon experiments.

Of particular interest is the latest generation of instruments, discussed above, which couple optical trapping with additional features. When combined with computer-driven, automated stages, optical traps can be used to sort and isolate a variety of items, including cells, sperm, and chromosomal fragments (20, 45). When combined with other laser techniques, such as optical scalpels, optical traps can assist in cellular

microsurgery (20). When combined with sensitive position sensors, optical traps can be turned into tensiometers capable of measuring minute forces and displacements (75, 78), or into novel imaging devices capable of nanometer-scale resolution (43). When combined with beam scanners, optical traps can be used to grasp, orient, and maneuver many objects simultaneously, facilitating their use in microfabrication and/or microchemistry (58–61, 67, 68, 84). Finally, new designs for optical traps (37), as well as the advent of low-cost diode lasers, may help to make this technology both more powerful and more accessible to the rest of the biological community.

ACKNOWLEDGMENTS

We thank Sarah Ali, Arthur Ashkin, Michael Burns, Christoph Schmidt, and Linda Turner for comments on the manuscript; Winfried Denk and William Wright for discussions; Catherine Hirshfeld for help in preparing Table 1; Tom Deutsch and Kevin Schomacker for the data of Figure 3; Karl Aufderheide, Lucien Ghislain, Hiroaki Misawa, Mara Prentiss, William Wright, and Koen Visscher for sharing results in advance of publication; and the Rowland Institute for Science for supporting this work.

Literature Cited

1. Ashkin A. 1970. Acceleration and trapping of particles by radiation pressure. *Phys. Rev. Lett.* 24:156–59
2. Ashkin A. 1971. Optical levitation by radiation pressure. *Appl. Phys. Lett.* 19: 283–85
2a. Ashkin A. 1978. Trapping of atoms by resonance radiation pressure. *Phys. Rev. Lett.* 40:729–32
3. Ashkin A. 1980. Applications of laser radiation pressure. *Science* 210:1081–88
4. Ashkin A. 1992. Forces of a single-beam gradient laser trap on a dielectric sphere in the ray optics regime. *Biophys. J.* 61: 569–82
5. Ashkin A, Dziedzic JM. 1975. Optical levitation of liquid drops by radiation pressure. *Science* 187:1073–75
6. Ashkin A, Dziedzic JM. 1976. Optical levitation in high vacuum. *Appl. Phys. Lett.* 28:333–35
7. Ashkin A, Dziedzic JM. 1987. Optical trapping and manipulation of viruses and bacteria. *Science* 235:1517–20
8. Ashkin A, Dziedzic JM. 1989. Optical trapping and manipulation of single cells using infra-red laser beams. *Ber. Busenges. Phys. Chem.* 93:254–60
9. Ashkin A, Dziedzic JM. 1989. Internal cell manipulation using infrared laser traps. *Proc. Natl. Acad. Sci. USA* 86: 7914–18
10. Ashkin A, Dziedzic JM, Bjorkholm JE, Chu S. 1986. Observation of a single-beam gradient force optical trap for dielectric particles. *Opt. Lett.* 11:288–90
11. Ashkin A, Dziedzic JM, Yamane T. 1987. Optical trapping and manipulation of single cells using infrared laser beams. *Nature* 330:769–71
12. Ashkin A, Schuetze K, Dziedzic JM, Euteneuer U, Schliwa M. 1990. Force

generation of organelle transport measured in vivo by an infrared laser trap. *Nature* 348:346–48
13. Aufderheide KJ, Du Q, Fry ES. 1992. Directed positioning of nuclei in living *Paramecium tetraurelia:* use of the laser optical force trap for developmental biology. *Dev. Genet.* 13:235–40
14. Aufderheide KJ, Du Q, Fry ES. 1993. Directed positioning of micronuclei in *Paramecium tetraurelia* with laser tweezers: absence of detectable damage after manipulation. *J. Eukaryot. Microbiol.* 40:793–96
15. Bakker Schut TC, Hesselink G, de Grooth BG, Greve J. 1991. Experimental and theoretical investigations on the validity of the geometrical optics model for calculating the stability of optical traps. *Cytometry* 12:479–85
16. Barton JP, Alexander DR. 1989. Fifth-order corrected electromagnetic field components for a fundamental Gaussian beam. *J. Appl. Phys.* 66:2800–2
17. Barton JP, Alexander DR, Schaub SA. 1988. Internal and near-surface electromagnetic fields for a spherical particle irradiated by a focused laser beam. *J. Appl. Phys.* 64:1632–39
18. Barton JP, Alexander DR, Schaub SA. 1989. Theoretical determination of net radiation force and torque for a spherical particle illuminated by a focused laser beam. *J. Appl. Phys.* 66:4594–4602
19. Berns MW, Aist JR, Wright WH, Liang H. 1992. Optical trapping in animal and fungal cells using a tunable, near-infrared titanium-sapphire laser. *Exp. Cell Res.* 198:375–78
20. Berns MW, Wright WH, Steubing, RW. 1991. Laser microbeam as a tool in cell biology. *Int. Rev. Cytol.* 129:1–44
21. Berns MW, Wright WH, Tromberg BJ, Profeta GA, Andrews JJ, Walter RJ. 1989. Use of laser-induced optical force trap to study chromosome movement on the mitotic spindle. *Proc. Natl. Acad. Sci. USA* 86:4539–43
22. Block SM. 1990. Optical tweezers: a new tool for biophysics. In *Noninvasive Techniques in Cell Biology (Mod. Rev. Cell Biol. 9)*, ed. JK Foskett, S Grinstein, 15:375–402. New York: Wiley-Liss. 423 pp.
23. Block SM. 1992. Making light work with optical tweezers. *Nature* 360:493–95
24. Block SM, Blair DF, Berg HC. 1989. Compliance of bacterial flagella measured with optical tweezers. *Nature* 338:514–18
25. Block SM, Blair DF, Berg HC. 1991. Compliance of bacterial polyhooks measured with optical tweezers. *Cytometry* 12:492–96
26. Block SM, Goldstein LSB, Schnapp BJ. 1990. Bead movement by single kinesin molecules studied with optical tweezers. *Nature* 348:348–52
27. Brennen C, Winet H. 1977. Fluid mechanics of propulsion by cilia and flagella. *Annu. Rev. Fluid Mech.* 9:339–98
28. Buican TN, Neagley DL, Morrison WC, Upham BD. 1989. Optical trapping, cell manipulation, and robotics. *SPIE New Technol. Cytometry* 1063: 190–97
29. Buican TN, Smyth MJ, Crissman HA, Salzman GC, Stewart CC, Martin JC. 1987. Automated single-cell manipulation and sorting by light trapping. *Appl. Opt.* 26:5311–16
30. Burns MM, Fournier J-M, Golovchenko JA. 1989. Optical binding. *Phys. Rev. Lett.* 63:1233–36
31. Burns MM, Fournier J-M, Golovchenko JA. 1990. Optical matter: crystallization and binding in intense optical fields. *Science* 249:749–54
32. Charon NW, Goldstein SF, Block SM, Curci K, Ruby JD, et al. 1992. Morphology and dynamics of protruding spirochete periplasmic flagella. *J. Bacteriol.* 174:832–40
33. Chu S. 1991. Laser manipulation of atoms and particles. *Science* 253:861–66
34. Chu S. 1992. Laser trapping of neutral particles. *Sci. Am.* 266;2:49–54
35. Chu S, Kron SJ. 1992. Method for optically manipulating polymer filaments. *US Patent #5079169*
36. Colon, JM, Sarosi PG, McGovern PG, Ashkin A, Dziedzic JM, et al. 1992. Controlled micromanipulation of human sperm in three dimensions with an infrared laser optical trap: effect on sperm velocity. *Fertil. Steril.* 57:695–98
37. Constable A, Kim J, Mervis J, Zarinetchi Z, Prentiss M. 1993. Demonstration of a fiber-optical light-force trap. *Opt. Lett.* 18:1867–69
38. Davis LW. 1979. Theory of electromagnetic beams. *Phys. Rev. A* 19: 1177–79
39. Denk W, Webb WW. 1990. Optical measurements of picometer displacements of transparent microscopic objects. *Appl. Opt.* 29:2382–90
40. Edidin M, Kuo SC, Sheetz MP. 1991. Lateral movements of membrane glycoproteins restricted by dynamic cytoplasmic barriers. *Science* 254:1379–82
41. Garnaes G, Schwartz DK, Viswanathan R, Zasadzinski JAN. 1992. Domain boundaries and buckling superstruc-

tures in Langmuir-Blodgett films. *Nature* 357:54–57
42. Gelles J, Schnapp BJ, Sheetz MP. 1988. Tracking kinesin-driven movements with nanometer-scale precision. *Nature* 331:450–53
43. Ghishlain LP, Webb WW. 1993. Scanning force microscopy using an optical trap. *Opt. Lett.* 18:1678–80
44. Gordon JP. 1973. Radiation forces and momenta in dielectric media. *Phys. Rev. A* 8:14–21
45. Greulich KO. 1992. Chromosome microtechnology: microdissection and microcloning. *Trends Biotechnol.* 10:48–51
46. Greulich KO, Weber G. 1991. The laser microscope on its way from an analytical to a preperative tool. *J. Microsc.* 167:127–51
47. Grimbergen J, Visscher K, Gomes de Mesquita D. 1993. Isolation of single yeast cells by optical trapping. *Yeast* 9: 723–32
47a. Gussgard R, Lindmo T, Brevik I. 1992. Calculation of trapping force in a strongly focused laser beam. *J. Opt. Soc. Am.* 9:1922–30
48. Happel J, Brenner H. 1991. *Low Reynolds Number Hydrodynamics.* Dordecht, the Netherlands: Kluwer Academic. 2nd ed. 553 pp.
49. Jackson JD. 1975. *Classical Electrodynamics,* p. 239. New York, NY: Wiley. 2nd ed.
50. Kamimura S. 1987. Direct measurements of nanometric displacements under an optical microscope. *Appl. Opt.* 26:3425–27
51. Kamimura S, Kamiya R. 1992. High-frequency vibration in flagellar axonemes with amplitudes reflecting the size of tubulin. *J. Cell Biol.* 116:1443–54
52. Kerker M. 1969. *The Scattering of Light and Other Electromagnetic Radiation,* pp. 32–37. New York, NY: Academic. 666 pp.
53. Kucik DF, Kuo SC, Elson EL, Sheetz MP. 1991. Preferential attachment of membrane glycoproteins to the cytoskeleton at the leading edge of lamella. *J. Cell Biol.* 114:1029–36
54. Kuo SC, Sheetz MP. 1992. Optical tweezers in cell biology. *Trends Cell Biol.* 2:116–18
55. Kuo SC, Sheetz MP. 1993. Force of single kinesin molecules measured with optical tweezers. *Science* 260:232–34
56. Liang H, Wright WH, He W, Berns MW. 1991. Micromanipulation of mitotic chromosomes in PTK-2 cells using laser-induced optical forces ("optical tweezers"). *Exp. Cell Res.* 197:21–35
57. Liang H, Wright WH, He W, Berns MW. 1993. Micromanipulation of chromosomes in PTK-2 cells using laser microsurgery (optical scalpel) in combination with laser-induced optical force (optical tweezers). *Exp. Cell Res.* 204: 110–20
58. Misawa H, Koshioka M, Sasaki K, Kitamura N, Masuhara H. 1990. Laser trapping, spectroscopy, and ablation of a single latex particle in water. *Chem. Lett. Japan* pp. 1479–82
59. Misawa H, Koshioka M, Sasaki K, Kitamura N, Masuhara H. 1991. Spatial pattern formation, size selection, and directional flow of polymer latex particles by laser trapping technique. *Chem. Lett. Japan* pp. 469–72
60. Misawa H, Koshioka M, Sasaki K, Kitamura N, Masuhara H. 1991. Three-dimensional optical trapping and laser ablation of a single polymer latex particle in water. *J. Appl. Phys.* 70:3829–36
61. Misawa H, Sasaki K, Koshioka M, Kitamura N, Masuhara H. 1992. Multibeam laser manipulation and fixation of microparticles. *Appl. Phys. Lett.* 60: 310–12
61a. Papoulis A. 1977. *Signal Analysis.* New York, NY: McGraw-Hill. 431 pp.
62. Purcell EM, Pennypacker CR. 1973. Scattering and absorption of light by nonspherical dielectric grains. *Astrophys. J.* 186:705–14
63. Radmacher M, Tillmann RW, Fritz M, Gaub HE. 1992. From molecules to cells: imaging soft samples with the atomic force microscope. *Science* 257: 1900–5
64. Richards B, Wolf E. 1959. Electromagnetic diffraction in optical systems. II. Structure of the image field in an aplanatic system. *Proc. R. Soc. London Ser. A* 253:358–79
65. Roosen G. 1979. La lévitation optique de sphères. *Can. J. Phys.* 57:1260–79
66. Roosen G, Imbert C. 1976. Optical levitation by means of two horizontal laser beams: a theoretical and experimental study. *Physics Lett.* 59A:6–8
67. Sasaki K, Koshioka M, Misawa H, Kitamura N, Masuhara H. 1991. Laser-scanning micromanipulation and spatial patterning of fine particles. *Jpn. J. Appl. Phys.* 30:907–909
68. Sasaki K, Koshioka M, Misawa H, Kitamura N, Masuhara H. 1992. Optical trapping of a metal particle and a water droplet by a scanning laser beam. *Appl. Phys. Lett.* 60:807–9
69. Sato S, Ohyumi M, Shibata H, Inaba H. 1991. Optical trapping of small particles using a 1.3-micrometer compact In-

GaAsp diode laser. *Opt. Lett.* 16:282–84

70. Schneider M, Webb WW. 1981. Measurement of submicron laser beam radii. *Appl. Opt.* 20:1382–88
71. Seeger S, Manojembashi S, Hutter K-J, Futterman G, Wolfrum J, Greulich KO. 1991. Application of laser optical tweezers in immunology and molecular genetics. *Cytometry* 12:497–504
72. Shepherd GMG, Corey DP, Block SM. 1990. Actin cores of hair-cell stereocilia support myosin movement. *Proc. Natl. Acad. Sci.* USA 87:8627–31
73. Siegmann AE. 1986. *Lasers.* Mill Valley, CA: University Science. 1283 pp.
74. Simmons RM, Finer JT. 1993. Glasperlenspiel II: optical tweezers. *Curr. Biol.* 3:309–11
75. Simmons RM, Finer JT, Warrick HM, Kralik B, Chu S, Spudich JA. 1993. Force on single actin filaments in a motility assay measured with an optical trap. In *The Mechanism of Myofilament Sliding in Muscle Contraction,* ed. H Sugi, GH Pollack, pp. 331–36. New York, NY: Plenum
76. Steubing, RW, Cheng S, Wright WH, Numajiri Y, Berns MW. 1991. Laser induced cell fusion in combination with optical tweezers: the laser cell fusion trap. *Cytometry* 12:505–10
77. Svoboda K, Schmidt CF, Branton D, Block SM. 1992. Conformation and elasticity of the isolated red blood cell membrane skeleton. *Biophys. J.* 63: 784–93
78. Svoboda K, Schmidt CF, Schnapp BJ, Block SM. 1993. Direct observation of kinesin stepping by optical trapping interfcrometry. *Nature* 365:721–27
79. Tadir Y, Wright WH, Vafa O, Ord T, Asch RH, Berns MW. 1990. Force generated by human sperm correlated to velocity and determined using a laser generated optical trap. *Fertil. Steril.* 53: 944–47
80. Visscher K. 1993. *Optical manipulation and confocal microscopy,* pp. 73–77. PhD thesis, University of Amsterdam, Netherlands. 115 pp.
81. Visscher K, Brakenhoff GJ. 1991. Single beam optical trapping integrated in a confocal microscope for biological applications. *Cytometry* 12:486–91
82. Visscher K, Brakenhoff GJ. 1992. Theoretical study of optically induced forces on spherical particles in a single beam trap I: Rayleigh scatterers. *Optik* 89: 174–80
83. Visscher K, Brakenhoff GJ. 1992. Theoretical study of optically induced forces on spherical particles in a single beam trap II: Mie scatterers. *Optik* 90:57–60
84. Visscher K, Brakenhoff GJ, Krol JJ. 1993. Micromanipulation by "multiple" optical traps created by a single fast scanning trap integrated with the bilateral confocal scanning microscope. *Cytometry* 14:105–14
85. Vorobjev IA, Liang H, Wright WH, Berns MW. 1993. Optical trapping for chromosome manipulation: a wavelength dependence of induced chromosome bridges. *Biophys. J.* 64:533–38
86. Wang MC, Uhlenbeck, GE. 1945. On the theory of the Brownian motion II. *Rev. Mod. Phys.* 17:323–41; Reprinted in *Selected Papers on Noise and Stochastic Processes,* ed. N Wax, pp. 113–32. New York, NY: Dover
87. Warrick HM, Simmons RM, Finer JT, Uyeda TQP, Chu S, Spudich JA. 1993. In vitro methods for measuring force and velocity of the actin-myosin interaction using purified proteins. *Methods Cell Biol.* 39:1–21
88. Weber G, Greulich KO. 1992. Manipulation of cells, organelles, and genomes by laser microbeam and optical trap. *Int. Rev. Cytol.* 133:1–41
89. Weisenhorn AL, Hansma PK, Albrecht TR, Quate CF. 1989. *Appl. Phys. Lett.* 54:2651–53
90. Wright WH, Sonek GJ, Berns, MW. 1993. Radiation trapping forces on microspheres with optical tweezers. *Appl. Phys. Lett.* 63:715–17
91. Wright WH, Sonek GJ, Berns, MW. 1993. A parametric study of the forces on microspheres held by optical tweezers. *Appl. Opt.* In press
92. Wright WH, Sonek GJ, Tadir Y, Berns MW. 1990. Laser trapping in cell biology. *IEEE J. Quantum Electron.* 26: 2148–57
93. Wu J. 1991. Acoustical tweezers. *J. Acoust. Soc. Am.* 89:2140–43

Annual Review of Biophysics and Biomolecular Structure
Volume 23, 1994

CONTENTS

vi (*continued*)